J. Fluid Mech. (2007), *vol.* 570, *pp.* 347–364. © 2007 Cambridge University Press
doi:10.1017/S0022112006003107 Printed in the United Kingdom

Direct numerical simulation of hypersonic turbulent boundary layers. Part 1. Initialization and comparison with experiments

By M. PINO MARTIN

Mechanical and Aerospace Engineering Department, Princeton University, Princeton, NJ 08544, USA

(Received 4 November 2004 and in revised form 24 April 2006)

A systematic procedure for initializing supersonic and hypersonic turbulent boundary layers at controlled Mach number and Reynolds number conditions is described. The initialization is done by locally transforming a true direct numerical simulation flow field, and results in a nearly realistic initial magnitude of turbulent fluctuations, turbulence structure and energy distribution. The time scales necessary to forget the initial condition are studied. The experimental conditions of previous studies are simulated. The magnitude of velocity and temperature fluctuations, as well as the turbulent shear stresses given by the direct numerical simulations are in agreement with the experimental data.

1. Introduction

The study of high-speed boundary layers is important in advancing supersonic and hypersonic flight technology. In a high-speed boundary layer, the kinetic energy is substantial and the dissipation due to the presence of the wall leads to a large increase in temperature. Therefore, a high-speed boundary layer differs from an incompressible one in that the temperature gradients are significant. Since the pressure remains nearly constant across the boundary layer, the density decreases where the temperature increases. Thus, to accommodate for an equivalent mass-flux, a supersonic boundary layer must grow faster than a subsonic one. The extra growth modifies the free stream, and the interaction between the inviscid free stream and the viscous boundary layer affects the wall-pressure distribution, the skin friction and the heat transfer. Furthermore, the high temperature in the boundary layer leads to air reactions. To improve our understanding of the flow physics and to calibrate turbulence models, we need accurate experimental and computational databases of high-speed turbulent boundary layers.

Direct numerical simulations (DNSs) provide a large amount of accurate data that can be used to analyse turbulent boundary layers at high Mach numbers. Based on a better understanding of the real flow physics and using DNS data, accurate turbulence models for high-speed flows can be developed, calibrated and tested. Recent advances show that building a detailed DNS database of fundamental flows at supersonic and hypersonic conditions is attainable. For example, Guarini *et al.* (2000) perform a DNS of a Mach 2.5 boundary layer at $Re_\theta = 1577$; Adams (2000) performs a DNS of the turbulent boundary layer over a compression ramp at Mach 3 and $Re_\theta = 1685$; Martin & Candler (2001) perform DNS of turbulent boundary layers at Mach 4 and $\mathrm{Re}_\theta = 7225$ and 9480 with different wall temperatures; Xu & Martin (2003, 2004) study the effect of inflow conditions in compressible turbulent boundary

layers with Re_θ up to 12 800; and Martin & Candler (2000, 2001) perform DNS of reacting boundary layers at Mach 4. One of the achievements of the DNS work is the ability to simulate turbulent flows at high Mach numbers accurately while reproducing complex flow physics, permitting the study of turbulence under different flow conditions.

In this work, we present an initialization procedure to minimize simulation transients, while matching the desired Mach number, Reynolds number and skin friction. We describe the evolution from the initial condition to the realistic turbulence state. We demonstrate that the initialization procedure is cost effective and that it allows for controlled flow conditions, which is necessary for one-to-one comparisons against experimental data. In addition, the initialization procedure and the DNS data are validated by comparison against the experimental data of Debiéve, Gouin & Faviglio (1981), Debiéve (1983), Eléna, Lacharme & Gaviglio (1985) and Eléna & Lacharme (1988).

The paper is organized as follows. Sections 2 and 3 describe the governing equations and the numerical method. The initialization procedure is derived in § 4. Details of the resolution requirements and flow conditions are given in § 5. The DNS data are assessed in § 6, including comparison against experiments. Conclusions are given in § 7.

2. Governing equations

The equations describing the unsteady motion of a perfect gas flow are given by the mass, momentum and total energy conservation equations

$$\frac{\partial \rho}{\partial t} + \frac{\partial}{\partial x_j}(\rho u_j) = 0, \tag{2.1}$$

$$\frac{\partial \rho u_i}{\partial t} + \frac{\partial}{\partial x_j}(\rho u_i u_j + p\delta_{ij} - \sigma_{ij}) = 0, \tag{2.2}$$

$$\frac{\partial \rho e}{\partial t} + \frac{\partial}{\partial x_j}((\rho e + p)u_j - u_i\sigma_{ij} + q_j) = 0, \tag{2.3}$$

where ρ is the density; u_j is the velocity in the j direction; p is the pressure; and σ_{ij} is the shear stress tensor given by a linear stress–strain relationship

$$\sigma_{ij} = 2\mu S_{ij} - \tfrac{2}{3}\mu\delta_{ij}S_{kk}, \tag{2.4}$$

where $S_{ij} = (\partial u_i/\partial x_j + \partial u_j/\partial x_i)/2$, is the strain rate tensor, μ is the temperature-dependent viscosity and is computed using a power law; and q_j is the heat flux due to temperature gradients

$$q_j = -\kappa\frac{\partial T}{\partial x_j}, \tag{2.5}$$

where κ is the temperature-dependent thermal conductivity; and e is the total energy per unit mass given by

$$e = c_v T + \tfrac{1}{2}u_i u_i, \tag{2.6}$$

where c_v is the assumed constant specific heat at constant volume.

3. Numerical method

The numerical method combines a weighted essentially non-oscillatory (WENO) scheme for the inviscid fluxes with an implicit time-advancement technique. The third-order-accurate bandwidth-optimized WENO scheme (Weirs & Candler 1997;

Martin *et al.* 2006) was designed for low dissipation and high bandwidth and provides shock-capturing, which is necessary at the Mach numbers that we consider. The time-advancement technique is based on the data-parallel lower-upper relaxation (DP-LUR) method of Candler, Wright & McDonald (1994), which has been extended to second-order accuracy and validated for compressible turbulence (Martin & Candler 2006). The derivatives required for the viscous terms are evaluated using fourth-order central differences. The numerical code has been validated for the simulation of wall-bounded turbulent compressible flows (Martin 2004; Wu & Martin 2003, 2004; Xu & Martin 2004). We use supersonic boundary conditions in the free stream and periodic boundary conditions in the spanwise direction. As inflow conditions, we use either periodicity in the streamwise direction or prescribed inflow conditions (Xu & Martin 2003, 2004), which results in temporally developing (TDNS) or spatial simulations (SDNS), respectively. The validity of streamwise periodic boundary conditions is briefly discussed in this paper. A more detailed discussion can be found in Xu & Martin (2003, 2004).

4. Initialization procedure

To initialize the turbulent flow, we must prescribe the mean variables and their turbulent fluctuations. The mean flow can be obtained from theory or from a Reynolds-averaged Navier–Stokes (RANS) calculation with different degrees of accuracy depending on the flow conditions. Generally for DNS, the turbulent disturbances are prescribed using random-like perturbations with a flat frequency spectrum or white noise. Then, the initial flow is evolved to a realistic field in time, as the shape of the energy spectra and the turbulence structures develop into realistic ones.

The initial flow is considered transitional if we start with a laminar mean flow and small-magnitude perturbations. Then, we can obtain the desired Reynolds number by marching the initial flow field downstream during a DNS. This procedure is costly, depending on the desired final turbulent conditions. In contrast, if the initial mean flow is turbulent, we might reach a realistic turbulent flow field with a shorter simulation transient. The caveat here is that non-physically-prescribed-frequency-distributed perturbations lead to either uncontrolled final conditions (when the flow reaches realistic conditions at a higher-than-desired Reynolds number) or numerical instabilities that prevent the simulation from running. The former constraint increases with free-stream Mach number, as the nonlinear character of the governing equations is more apparent.

In the present work, we have developed an alternative procedure to initialize the simulations at the desired conditions, matching Mach number, Reynolds number and boundary conditions. The resulting initial turbulent fields have nearly realistic attributes: mean flow, statistics, energy spectra and local turbulence structure. In turn, the simulation transients are short, and the turbulence conditions at the onset of realistic turbulence can be controlled.

Figure 1 plots a schematic of the initialization procedure. We first obtain the mean turbulent flow using a Baldwin–Lomax Reynolds-averaged Navier–Stokes simulation (Wright 2003). The RANS mean flow carries the Mach, Re_θ, and boundary condition information. We obtain the fluctuating velocity field by locally transforming the turbulence field of a DNS at $M = 0.3$ (Spalart 1988). Finally, we use the strong Reynolds analogy (Morkovin 1962) to calculate the fluctuations in the thermodynamic variables. Details of this procedure are given below.

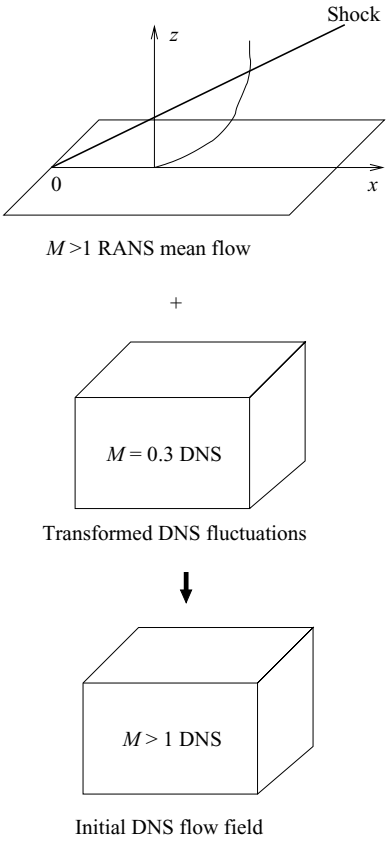

FIGURE 1. Schematic of the initialization procedure for the direct numerical simulation of turbulent boundary layers.

Case	M_∞	ρ_∞ (kg m^{-3})	T_∞ (K)	T_w/T_∞	Re_θ
M3	3.00	0.0889	216.65	2.66	2297
M4	4.00	0.0889	216.65	3.88	3767
M5	5.00	0.0889	216.65	5.50	5392
M6	6.00	0.0889	216.65	7.48	7472

TABLE 1. Free-stream flow, wall-temperature, and boundary layer profile conditions for the RANS calculations.

4.1. *Initial mean flow*

We perform RANS calculations of free-stream flow over a flat plate. Then, we select the mean flow at the desired Re_θ from the corresponding downstream location on the plate. Grid convergence studies are performed and the Van-Driest transformed velocity profiles, Reynolds number Re_θ, and the skin friction C_f are compared against the Van-Driest II predictions. Errors in these quantities are ironed out during the DNS simulation transient, which is longer with decreasing initial accuracy of the RANS mean flow profiles.

Table 1 gives the free-stream and wall-temperature conditions for the RANS calculations, as well as Re_θ for the mean profiles that are extracted from each

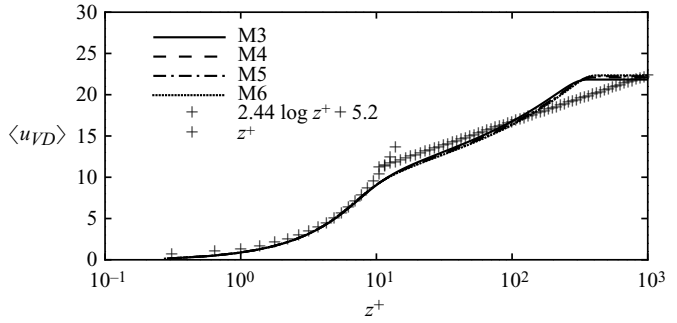

FIGURE 2. Initial mean velocity profiles from RANS.

calculation. Figure 2 shows the Van-Driest transformed velocity profiles given by the RANS calculations. The error in C_f relative to the Van-Driest II (Van-Driest 1956) predictions is less that 8 % for the calculations.

4.2. *Initial turbulence fluctuations*

To initialize the velocity fluctuations, we use the turbulent flow field of an incompressible DNS (Spalart 1988). We assume that (i) velocity fluctuations scale under the Morkovin transformation, and (ii) the near-wall turbulence structure is similar when visualized in wall units. These assumptions need not be true, they are simply used to obtain an estimate for the initial turbulent fluctuations. Then, the fluctuating velocity field is obtained by normalizing the local velocity fluctuations from the incompressible DNS using Morkovin's scaling and working in a computational domain that has also been normalized. Namely,

$$\sqrt{\frac{\overline{\rho}(z^*)}{\overline{\rho}_w}}\frac{u'(x^+, y^+, z^*)}{u_\tau}\Big|_{M>1} = \sqrt{\frac{\overline{\rho}(z^*)}{\overline{\rho}_w}}\frac{u'(x^+, y^+, z^*)}{u_\tau}\Big|_{M=0.3}, \tag{4.1}$$

where $\overline{\rho}_w$ is the mean density at the wall, x^+ and y^+ are the streamwise and spanwise directions, respectively, normalized in wall units, $z_\tau = u_\tau \rho/\mu$ where u_τ is the friction velocity; and z^* is the wall-normal direction, which is normalized in either wall units or outer units, i.e. the boundary-layer thickness δ, to give u'_{inner} or u'_{outer}, respectively. Then, the final local velocity fluctuation is calculated using

$$u'(x, y, z) = u'_{inner}(x, y, z)\,[1 - f(z)] + u'_{outer}(x, y, z)\,f(z), \tag{4.2}$$

where $f(z)$ is a hyperbolic-tangent function

$$f(z) = \frac{1}{2}\left\{1 + \tanh\left[4\left(\frac{z - z_{mid}}{z_{wake} - z_{log}}\right)\right]\right\} \tag{4.3}$$

with $z_{log} = 0.2\delta$, $z_{wake} = 0.5\delta$, and $z_{mid} = 0.5(z_{log} + z_{wake})$.

The initial fluctuations in the thermodynamic variables are estimated using the strong Reynolds analogy (Morkovin 1962) and assuming that pressure fluctuations are negligible in a turbulent boundary layer. Thus,

$$T' = -b(\gamma - 1)M^2\frac{u'}{\overline{u}}\overline{T}, \tag{4.4}$$

$$\frac{\rho'}{\overline{\rho}} = -\frac{T'}{\overline{T}}, \tag{4.5}$$

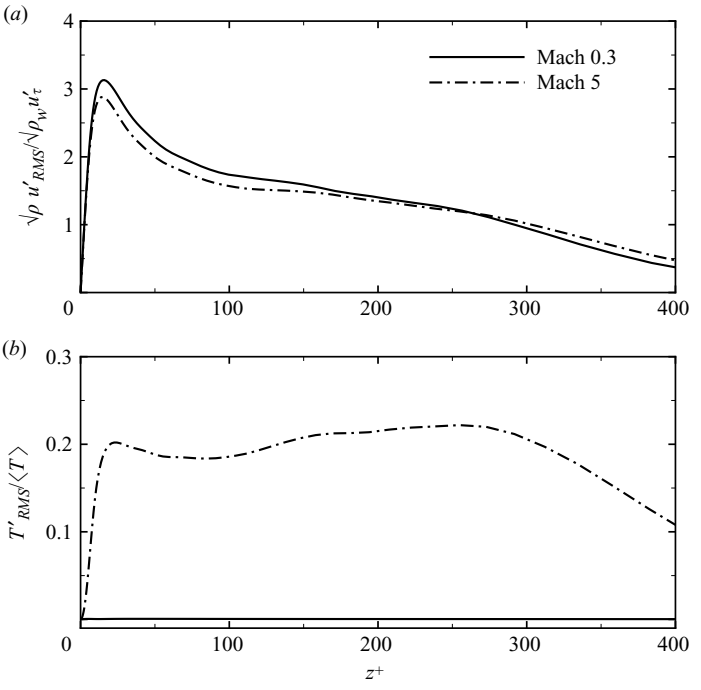

FIGURE 3. Initial velocity and temperature fluctuations for a Mach 5 turbulent boundary layer, case M5.

where $b = \min(0.8, b_{T>0})$ is a constant and conditional proportionality factor that ensures the positiveness of T everywhere in the flow field.

With this initial condition, the magnitude of the velocity fluctuations is realistic throughout the boundary layer. Because the transformation is done locally at each grid point and it starts with a true DNS flow field, the resulting initial turbulence structure and the corresponding energy distribution are nearly realistic. In the inner portion of the boundary layer, the structures are expected to be physically realistic. In the outer layer, however, the turbulence structure does not scale in wall units along the streamwise and spanwise directions, as suggested in (4.1), and therefore we do not expect a realistic representation of the local turbulence structure. However, we have a good guess at the entire flow field and as it is shown below, and the flow field adjusts during the simulation transient without altering the flow conditions significantly.

Figure 3(*a*) plots the Morkovin-scaled velocity fluctuations for the Mach 0.3 DNS and the initial flow field at Mach 5, M5. Figure 3(*b*) plots the magnitude of temperature fluctuations for the same cases. Temperature fluctuations are negligible for the Mach 0.3 case and non-zero for the Mach 5 case.

4.3. *Initial turbulent flow*

Combining the RANS mean profile with the transformed fluctuating field as described above leads to turbulent structures and energy spectra that resemble those of realistic turbulent boundary layers. Figure 4 plots contours of velocity for the Mach 0.3 DNS data and the initial turbulent field at Mach 5 at $z^+ = 8$. The streaky structure of the near-wall boundary layer is apparent. Figure 5 plots the energy spectra for the Mach 5 initial condition at $z^+ = 8$, and $z/\delta = 0.1$, 0.5 and 1.0. The energy is distributed in a cascade fashion, resembling that of a realistic turbulent flow.

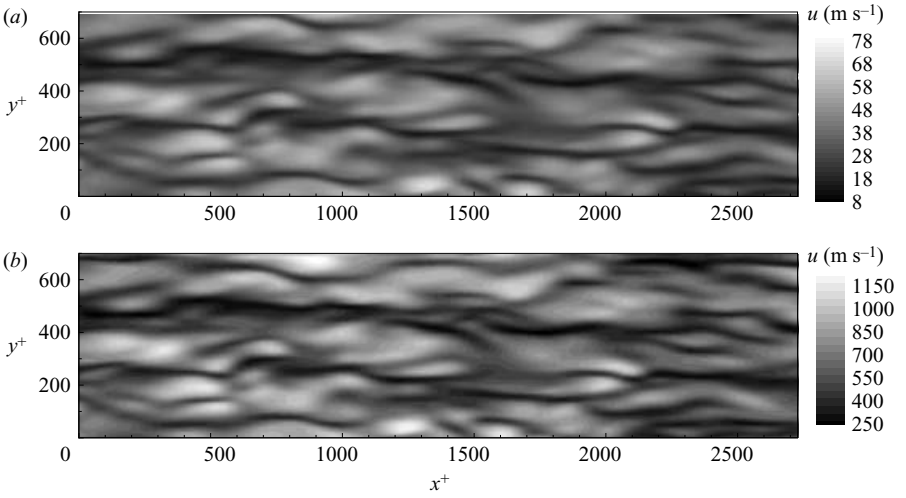

FIGURE 4. Velocity contours for the (*a*) Mach 0.3 and (*b*) initial Mach 5, case M5, boundary-layer flow field at $z^+ = 8$.

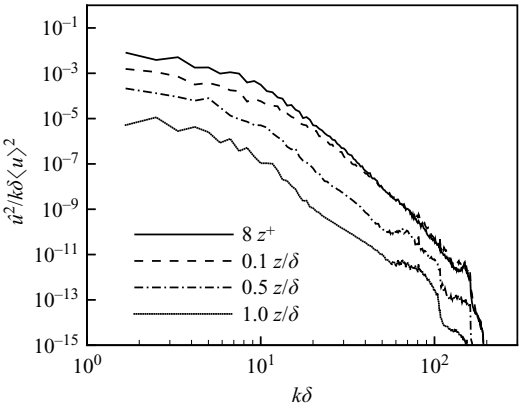

FIGURE 5. Initial energy spectra for a Mach 5 turbulent boundary layer, case M5.

5. DNS resolution requirements and flow conditions

The computational domain size and structured grid resolution required for the simulations is determined based on the large and small characteristic length scales, δ and z_τ, respectively. The computational domain must be large enough to contain a good sample of the large scales. On the other hand, the grid resolution must be fine enough to resolve the near-wall structures. The first requirement gives the size of the computational domain, whereas the latter one gives an estimate on the grid resolution in wall units. Thus, increasing the ratio of the large to small scale $\delta^+ = \delta/z_\tau$ increases the required number of grid points. Ultimately, grid convergence studies or comparisons with experimental or semi-empirical data will determine the final resolution.

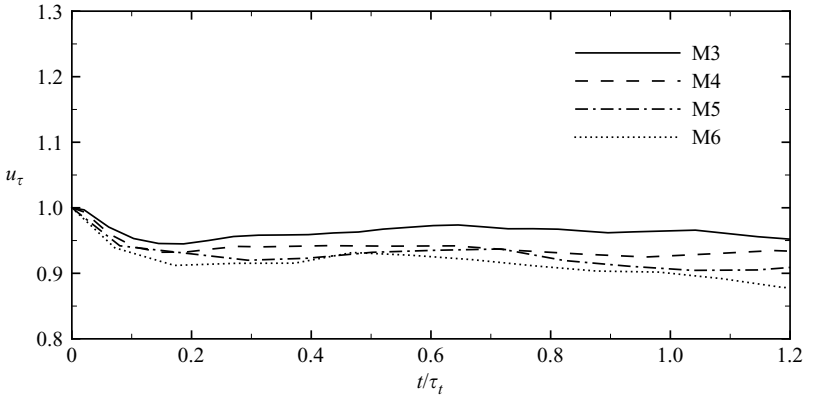

FIGURE 6. Temporal evolution of the friction velocity for the DNS of turbulent boundary layers.

After initializing the turbulent flow fields, we interpolate and/or apply periodicity when necessary to achieve the desired resolution and domain size.

6. Assessment of the DNS data

6.1. *Initialization transient and time scales*

We find that monitoring the temporal evolution of the friction velocity is a good indicator of the onset of equilibrium turbulence in the near-wall region. Figure 6(a) plots the normalized friction velocity versus time for the DNS. There is no appreciable variation in u_τ after about 0.2 non-dimensional time units, where t is non-dimensionalized by $\tau_t = \delta/u_\tau$ at $t = 0$. Figure 7 plots the temporal evolution of the energy spectra for the Mach 5 DNS. The energy distribution reaches equilibrium, as shown by the convergence of the data. For $z = 0.5\delta$, the energy takes about 1.5 non-dimensional time units to equilibrate. Figures 8(a) and 8(b) plot the magnitude of the normalized streamwise and wall-normal velocity fluctuations and figure 8(c) plots the magnitude of temperature fluctuations. We observe good convergence of the profiles. These results are representative of what is found in all cases.

To further corroborate the convergence time scales from above, we perturb the converged Mach 5 case by locally reducing the magnitude of the temperature fluctuations (by a half) and we consider the time it takes for the entire boundary layer to forget such a disturbance. Figure 9(a) plots the temporal evolution of T'_{RMS} profiles and figure 9(b) plots the temporal evolution of T'_{RMS} at selected wall-normal locations. For convenience, figure 9(c) plots the ratio of the local eddy turnover time, τ_Λ, to τ_t, where $\tau_\Lambda = \Lambda/u'_{RMS}$, with Λ as the integral length scale, which is computed from the spatio-temporal autocorrelation of u'. From these figures, the convergence rate of T'_{RMS} is about 0.2, 1.5 and 2 non-dimensional time units in the near wall, mid-layer and above, respectively, which is consistent with the previous results.

Once the boundary layer is in equilibrium, we gather statistics for one non-dimensional time unit, which corresponds to about 54, 45, 40 and 33 δ^*/U_δ units for cases M3 to M6, respectively, where δ^* and U_δ are the initial displacement thickness and the mean velocity at the boundary-layer edge, respectively. Figure 10 plots the Van-Driest transformed velocity profiles for the DNS database.

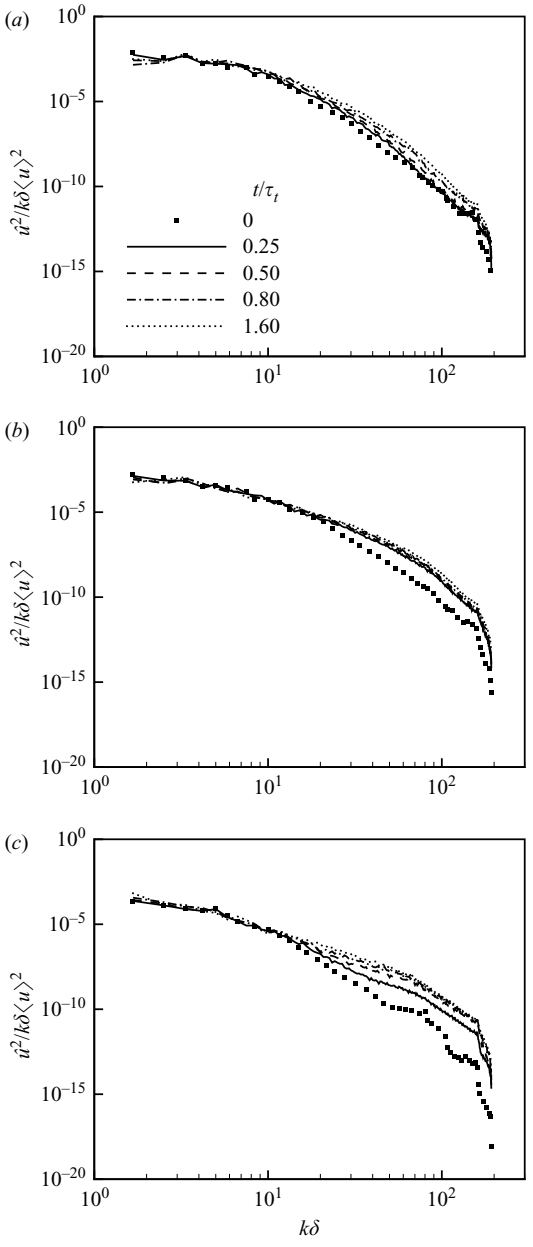

FIGURE 7. Non-dimensional energy spectra at (*a*) $z^+ = 8$, (*b*) $z/\delta = 0.1$ and (*c*) $z/\delta = 0.5$ for case M5.

6.2. *TDNS versus SDNS*

The amount of energy that is present in a supersonic boundary layer and the small streamwise computational lengths that are used in the present simulations, make it possible to use periodic boundary conditions in the streamwise direction. A time-developing boundary-layer simulation is valid provided that (i) the flow can be considered quasi-steady, i.e. the flow adjusts to its local (in time) conditions much

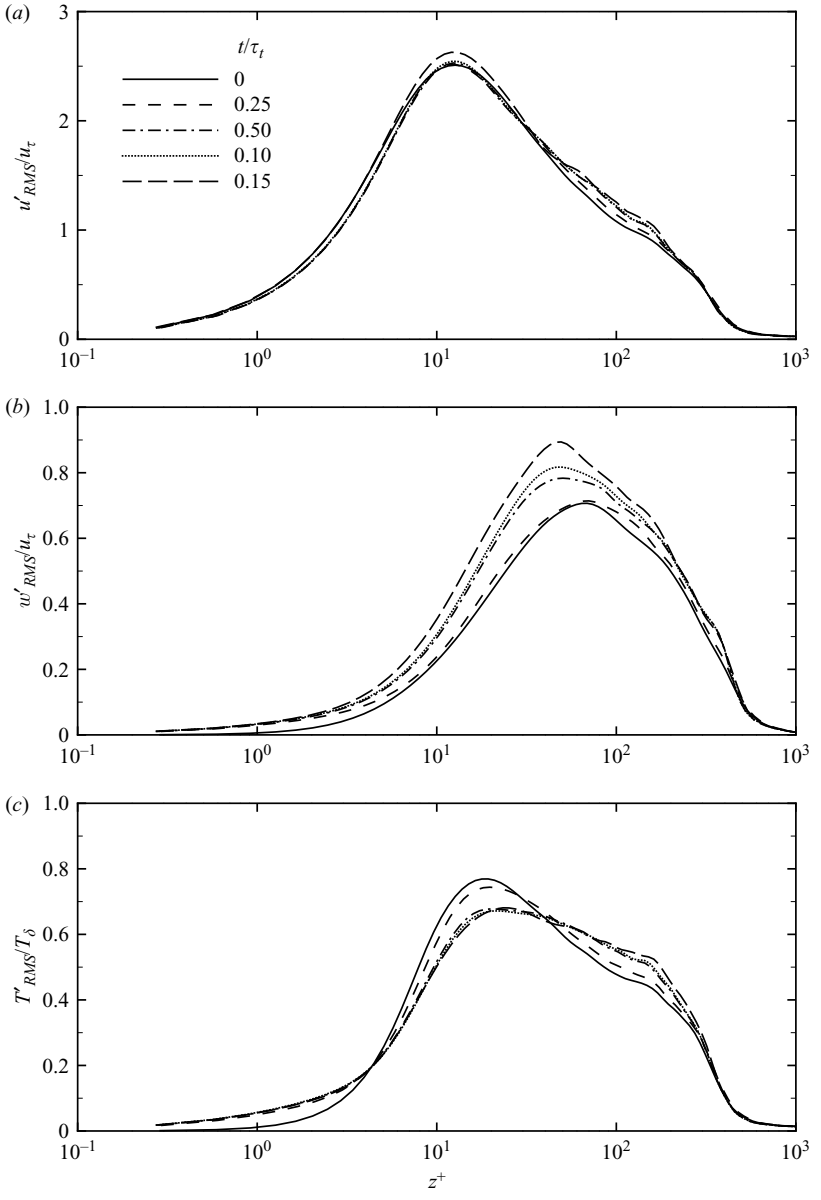

FIGURE 8. Normalized velocity fluctuations in the (*a*) streamwise and (*b*) wall-normal directions for case M5 and (*c*) normalized magnitude of temperature fluctuations.

faster than the boundary-layer thickness changes, and (ii) for the purposes of gathering statistics, the time sampling is shorter than the time scale for boundary-layer growth. A flow that satisfies these conditions evolves slowly and can be viewed as a good approximation of a static station of a boundary layer (Xu & Martin 2003, 2004).

The growth time, adjusting time, and sampling time can be estimated as

$$t_{growth} = \left(\frac{1}{\overline{\delta}}\frac{d\overline{\delta}}{dt}\right)^{-1}, \quad t_\delta = \frac{\overline{\delta}}{U_\delta}, \quad t_{sample} = \frac{\overline{\delta}}{\overline{u}_\tau},$$

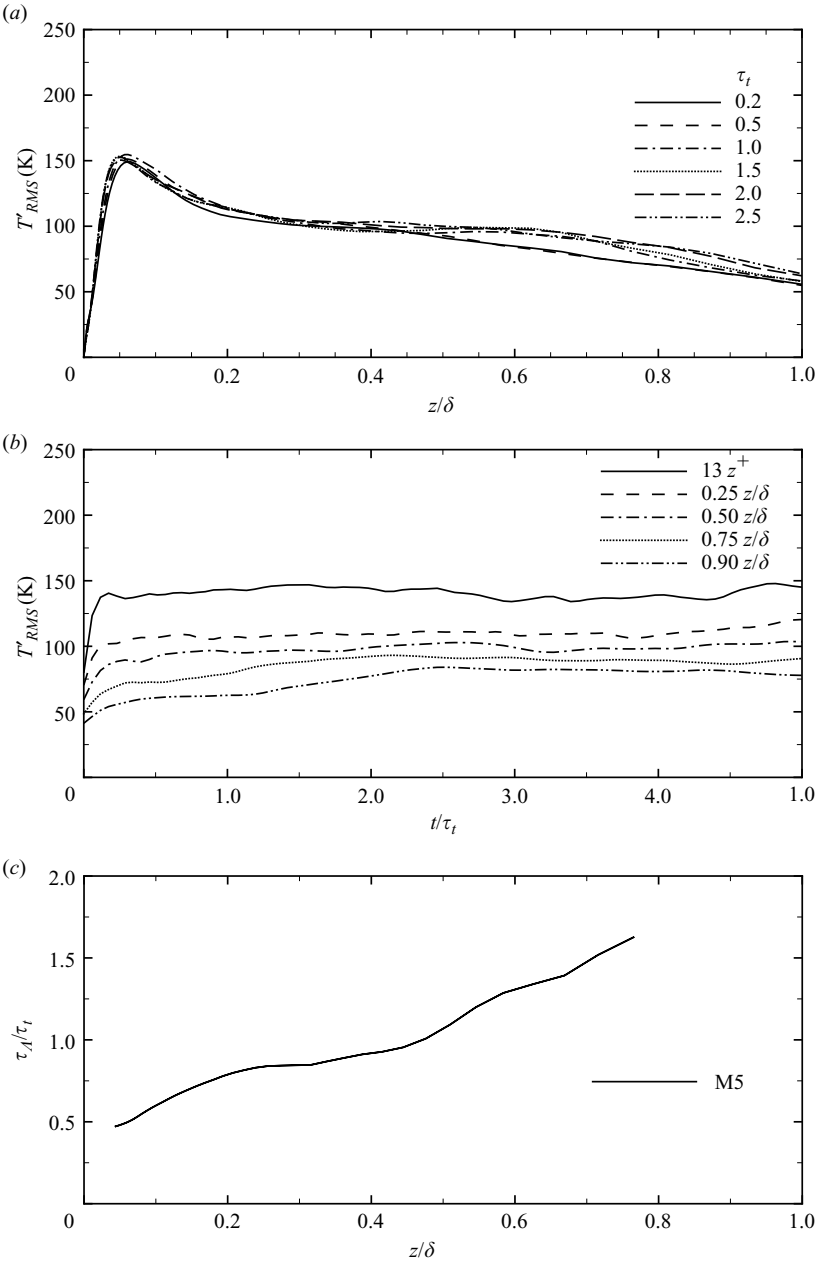

FIGURE 9. Temporal evolution of (*a*) T'_{RMS} profiles and (*b*) T'_{RMS} at selected wall-normal locations, and (*c*) ratio of τ_Λ to τ_t for a perturbed Mach 5 turbulent boundary layer from DNS.

respectively, where $\overline{\delta}$ and $\overline{u}_\tau$ are the averaged boundary-layer thickness and wall friction velocity. For the simulations, t_δ is at least two orders of magnitude smaller than t_{growth}, and t_{sample} is less than t_{growth}. Thus, the temporal development of the boundary layer is negligible during an appropriate data collection time. These premises are further corroborated below.

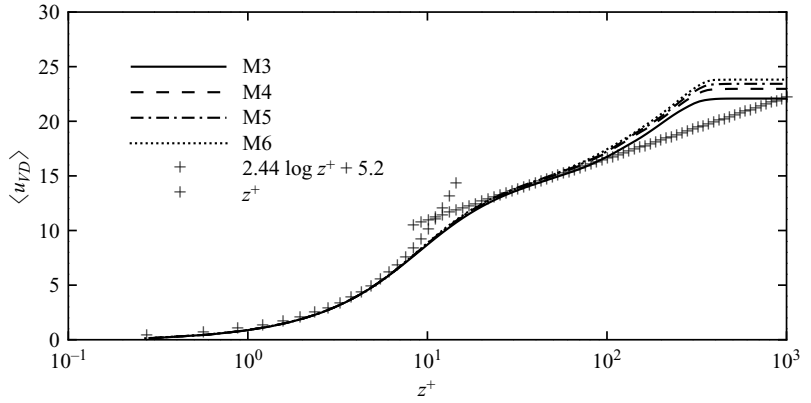

FIGURE 10. Mean velocity profiles for the DNS data.

Case	M_δ	ρ_δ (kg m^{-3})	T_δ (K)	T_w/T_δ	Re_θ	θ (mm)	H	δ (mm)
M3	2.98	0.0907	219.55	2.58	2390	0.430	5.4	6.04
M4	3.98	0.0923	219.69	3.83	3944	0.523	8.5	9.77
M5	4.97	0.0937	220.97	5.40	6225	0.657	12.2	14.82
M6	5.95	0.0952	221.49	7.32	8433	0.733	16.5	21.00

TABLE 2. Dimensional boundary-layer edge and wall parameters for the DNS database.

Case	δ^+	L_x/δ	L_y/δ	L_z/δ	Δx^+	Δy^+	N_x	N_y	N_z
M3	325	9.1	2.3	13.8	8.0	3.0	384	256	106
M4	368	7.9	2.0	15.4	7.6	2.8	384	256	110
M5	382	7.4	1.8	14.0	7.4	2.8	384	256	110
M6	396	7.0	1.7	15.3	7.2	2.7	384	256	112

TABLE 3. Grid resolution and domain size for the direct numerical simulations.

Figure 11(a) plots the temporal evolution of the friction velocity for case M5 using TDNS and SDNS. There is almost no difference between the two simulations. Figure 11(b) plots the temporal evolution of Re_θ. As expected, the Reynolds number is maintained during the spatial calculation. In contrast, Re_θ increases by roughly 25 % during the temporal simulation. Figure 11(c) plots the Van-Driest transformed velocity profiles for the same simulations. There is virtually no difference in the two datasets. Figure 11(d) plots the fluctuating Mach number. The second peak in the profile appears slightly farther from the wall for the TDNS simulations, which is a result of the increase in the Reynolds number during the simulation. For the conditions that we consider, the Reynolds number variation is not significant. All cases given in table 2 are computed with TDNS.

6.3. *Comparison with experimental data*

We consider the experimental flow conditions of Debiève (1983), Debiève *et al.* (1981) and Fernholz *et al.* (1989). The experiment includes the interaction of an $M = 2.32$,

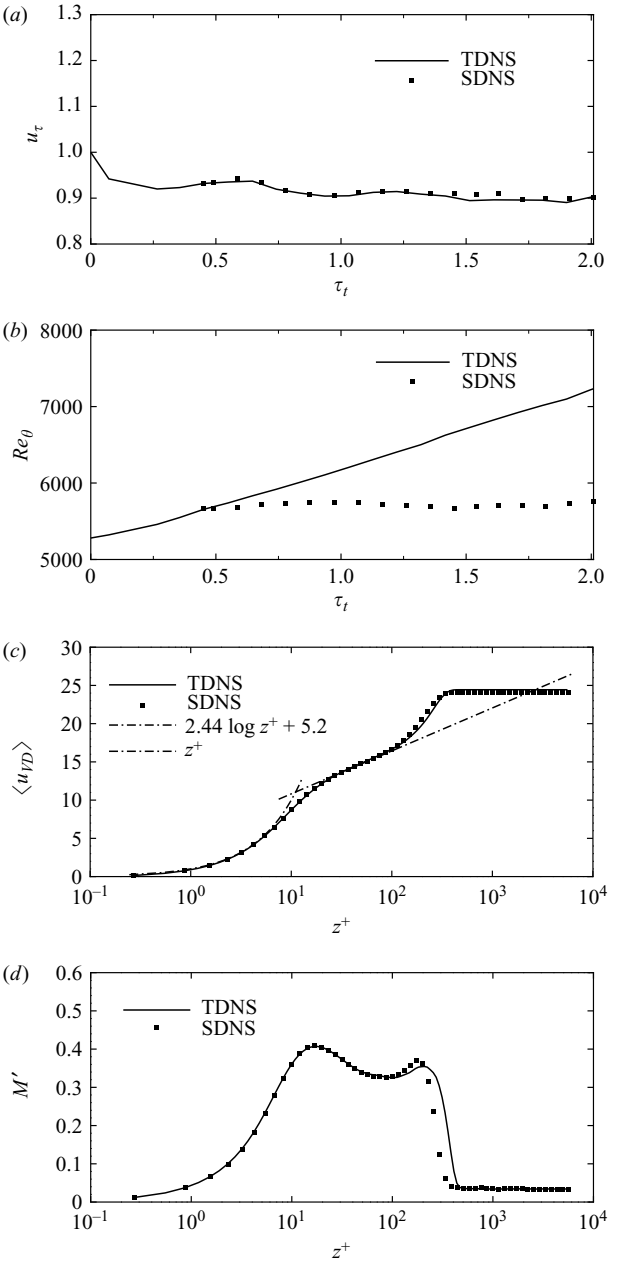

FIGURE 11. Comparison between TDNS and SDNS for case M5 (*a*) temporal evolution of the normalized friction velocity; (*b*) temporal evolution of Re_θ; (*c*) Van-Driest transformed velocity profile; (*d*) fluctuating Mach number.

$Re_\theta = 4000$ turbulent boundary layer with a shockwave along a compression corner. For validation, we use the experimental data for the boundary layer upstream of the interaction region. In the experiments, the magnitude of the velocity and temperature fluctuations are measured using constant-current hot-wire anemometry (CCA). Eléna *et al.* (1985) and Eléna & Lacharme (1988) perform experiments at nearly the same

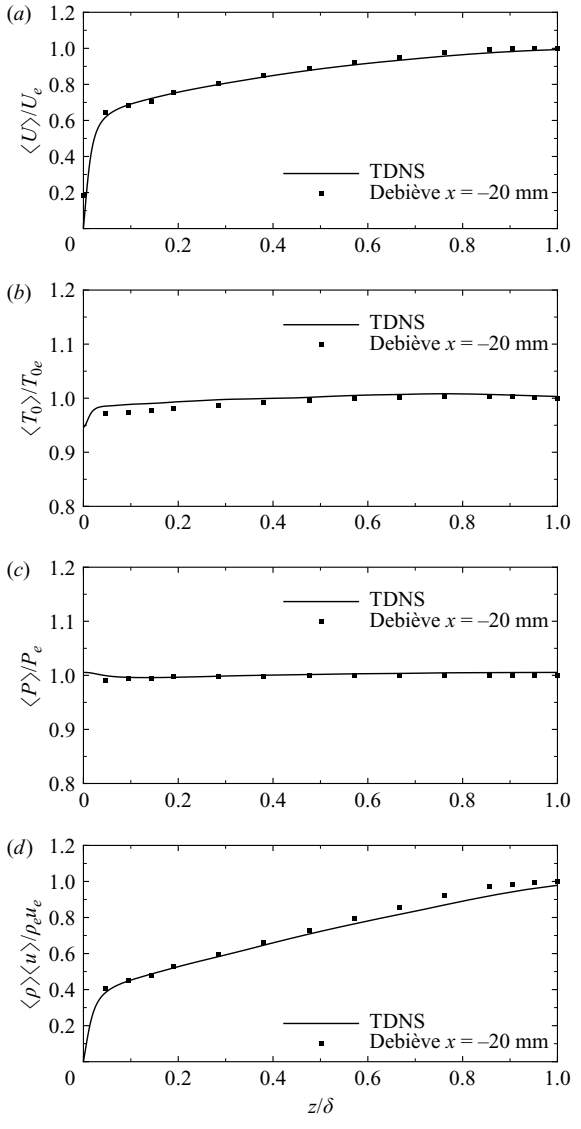

FIGURE 12. Comparison between DNS at $M = 2.32$ and $Re_\theta = 4450$ and experimental data (Debiéve 1981; Debiéve *et al.* 1983; Fernholz *et al.* 1989). Normalized values of mean (*a*) velocity; (*b*) total temperature; (*c*) pressure; (*d*) momentum. Quantities are normalized using edge values.

conditions with $M = 2.32$ and $Re_\theta = 4700$ and obtain measurements using laser-Doppler velocimetry (LDV) and CCA. They compare the data with the supersonic constant-temperature hot-wire anemometer (CTA) measurements of Johnson & Rose (1975), the supersonic experiments of Robinson, Seegmiller & Kussoy (1983), as well as the subsonic turbulent-boundary-layer study of Klebanoff (1955).

The DNS conditions are $M = 2.32$ and $Re_\theta = 4450$, where Re_θ is taken as an average value. Figure 12 plots the mean flow profiles for the DNS and experiments,

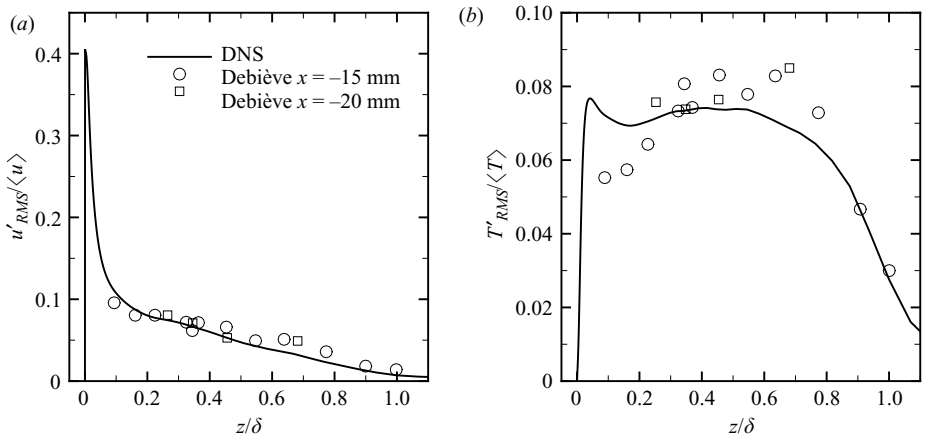

FIGURE 13. Comparison between DNS at $M = 2.32$ and $Re_\theta = 4450$ and experimental data (Debiéve 1981; Debiéve *et al.* 1983; Fernholz *et al.* 1989). (*a*) Streamwise component of turbulent fluctuations; (*b*) turbulent temperature fluctuations. Quantities are normalized using mean flow variables.

showing the good agreement among the data. Figures 13(*a*) and 13(*b*) plot the normalized magnitude of velocity and temperature fluctuations, respectively. The scatter in the data is within the experimental uncertainty. Figures 14(*a*) and 14(*b*) show the magnitude of the streamwise and wall-normal velocity fluctuations in comparison to the experiments of Eléna, where the data are normalized using the edge and friction velocities, respectively. The DNS data is in good agreement with the experimental measurements and within the scattered experimental data. Figure 14(*c*) plots the normalized turbulent shear stress, $\rho u'w'/\rho_w u_\tau^2$. Relative to Eléna's experiments, the DNS predicts increasingly higher values of the turbulent shear stress with decreasing distance from the wall. The DNS data also agrees well with the other supersonic and subsonic experimental data of Johnson & Rose (1975) and Robinson *et al.* (1983). Figure 14(*d*) plots the intermittency, where F_u is the flatness of velocity. The DNS gives higher intermittency levels. Figure 15 further illustrates the accuracy of the temperature field. The results of SDNS at $M = 2.32$ and maintained $Re_\theta = 4600$ are also shown. Figure 15(*a*) shows a test of the strong Reynolds analogy. The DNS and experimental data follow the trend of the modified analogy (Gaviglio 1987). Figure 15(*b*) shows the distribution of $-RuT$. The DNS data lie below the supersonic experimental data. Figure 15(*c*) plots the normalized magnitude of total temperature fluctuations. The DNS and experimental data differ in the boundary-layer edge region. Figures 12 to 15 illustrate the overall good agreement among the experimental and DNS data.

7. Conclusions

Studying physical phenomena via joint numerical and experimental databases requires controlled flow conditions. This presents a challenge for numerical simulations, since turbulent flows are highly nonlinear and initialization procedures

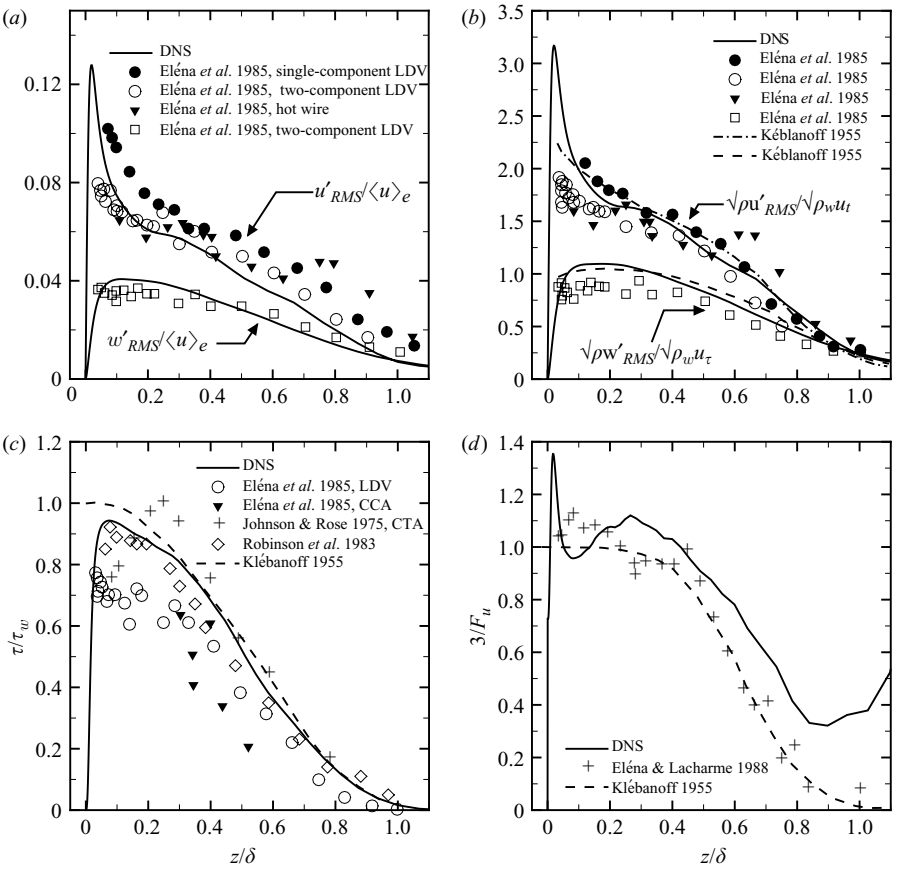

FIGURE 14. Comparison between DNS at $M = 2.32$ and $Re_\theta = 4450$ and experimental data (Klebanoff 1955; Elena *et al.* 1985; Elena & Lacharme 1988; Johnson & Rose 1975; Robinson *et al.* 1983). (*a*) Magnitude of velocity fluctuations normalized with edge velocity; (*b*) magnitude of velocity fluctuations normalized with Morkovin's scaling; (*c*) normalized turbulent shear stress; (*c*) intermittency factor.

and simulation transients make the final flow conditions difficult to control and costly to obtain if starting from a transitional boundary layer. In this paper, we have presented a local initialization procedure that leads to short simulation transients with nearly realistic initial magnitude of turbulence fluctuations, local turbulence structure and energy distribution. We have applied this procedure to initialize turbulent boundary layers over a large range of Reynolds number and Mach numbers. It has been shown that the procedure leads to controlled flow conditions. The time scales necessary for the flow to forget the initial condition are found to be about $0.2\tau_t$, $1.5\tau_t$, and $2\tau_t$ in the viscous sublayer, mid-layer and above regions, respectively. Using the new initialization procedure, we have simulated the experimental conditions of Debiève *et al.* (1981), Debiève (1983), Eléna *et al.* (1985) and Eléna & Lacharme (1988). The magnitude of velocity and temperature fluctuations, as well as the turbulent shear stresses given by the direct numerical simulations are in agreement with the experimental data.

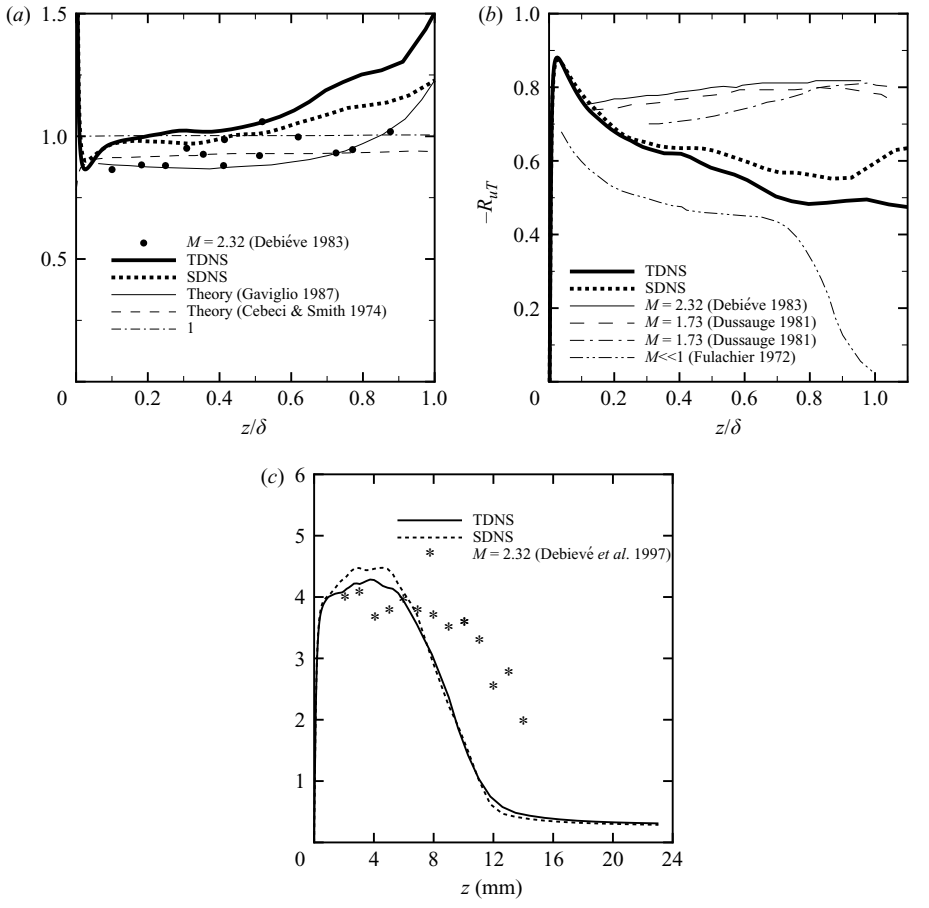

FIGURE 15. Comparison between DNS at $M = 2.32$ and $Re_\theta = 4450$ and experimental data. (*a*) Test of strong Reynolds analogy, $(T"_{rms}/\widetilde{u})/(\gamma - 1)M^2 u"_{rms}/\widetilde{u}$ where $\widetilde{u} = \overline{\rho}T/\overline{\rho}$ and $T" = T - \widetilde{u}$; (*b*) distribution of R_{uT}; (*c*) total temperature fluctuation distribution.

This work was supported by the Air Force Office of Scientific Research under grant AF/F49620-02-1-0361 and the National Science Foundation under grant CTS-0238390.

REFERENCES

ADAMS, N. 2000 Direct simulation of the turbulent boundary layer along a compression ramp at $M = 3$ and $Re_\theta = 1685$. *J. Fluid Mech.* **420**, 47–83.

CANDLER, G., WRIGHT, W. & MCDONALD, J. 1994 Data-parallel lower-upper relaxation method for reacting flows. *AIAA J.* **32**, 2380–2386.

CEBECI, T. & SMITH, A. M. O. 1974 *Analysis of Turbulent Boundary Layers*. Academic.

DEBIÈVE, J. 1983 Etude d'une interaction turbulence onde de choc. PhD thesis, Thèse Université d'Aix Marseille II.

DEBIÈVE, J., GOUIN, H. & GAVIGLIO, J. 1981 Momentum and temperature fluxes in a shock wave-turbulence interaction. *Proc. ICHMT/IUTAM Symp. on the Structure of Turbulence and Heat and Mass Transfer, Dubrovnik*.

Debiève, J.-F., Dupont, P., Smith, D. R. & Smits, A. J. 1997 Supersonic turbulent boundary layer subjected to step changes in wall temperature. *AIAA J.* **35**, 51–57.

Dussauge, J. P. 1981 Evolution de transferts turbulents dans une détente rapide, en écoulement supersonic. Doctorat es Sciences Physiques, I.M.S.T., Université d'Aix Marseille II.

Eléna, M. & Lacharme, J. 1988 Experimental study of a supersonic turbulent boundary layer using a laser Doppler anemometer. *J. Méc. Théor. Appl.* **7**, 175–190.

Eléna, M., Lacharme, J. & Gaviglio, J. 1985 Comparison of hot-wire and laser Doppler anemometry methods in supersonic turbulent boundary layers. In *Proc. Intl Symp. on Laser Anemometry* (ed. A. Dybb & P. A. Pfund). ASME.

Fernholz, H., Finley, P., Dussauge, J. & Smits, A. J. 1989 A survey of measurements and measuring techniques in rapidly distorted compressible turbulent boundary layers. *AGAR Dograph* 315.

Fulachier, L. 1972 "Contribution à l'étude des analogies des champs dynamiques et thermiques dans une couche limite turbulente. Effect de l'aspiration", Doctorat es Sciences Physiques, I.M.S.T., Université de Provence (Aix-Marseille).

Gaviglio, J. 1987 Reynolds analogies and experimental study of heat transfer in the supersonic boundary layer. *Intl J. Heat Mass Transfer* **30**, 911–926.

Guarini, S., Moser, R., Shariff, K. & Wray, A. 2000 Direct numerical simulation of supersonic turbulent boundary layer at Mach 2.5. *J. Fluid Mech.* **414**, 1–33.

Johnson, D. & Rose, W. 1975 Laser velocimetry and hot-wire anemometer comparison in a supersonic boundary layer. *AIAA J.* **13**, 512–515.

Klebanoff, P. 1955 Characteristics of turbulence in a boundary layer with zero pressure gradient. *NASA Rep.* 1247.

Martin, M. 2004 DNS of hypersonic turbulent boundary layers. *AIAA Paper* 2004-2337.

Martin, M. & Candler, G. 2000 DNS of a Mach 4 boundary layer with chemical reactions. *AIAA Paper* 2000-0399.

Martin, M. & Candler, G. 2001 Temperature fluctuation scaling in reacting boundary layers. *AIAA Paper* 2001-2717.

Martin, M. & Candler, G. 2006 A parallel implicit method for the direct numerical simulation of compressible flows. *J. Comput. Phys.* **215**, 153–171.

Martin, M., Taylor, E., Wu, M. & Weirs, V. 2006 A bandwidth-optimized WENO scheme for the direct numerical simulation of compressible turbulence. *J. Comput. Phys.* (accepted).

Morkovin, M. 1962 Effects of compressibility on turbulent flows. In *Mèchanique de la Turbulence*, pp. 367–380. CNRS.

Robinson, S., Seegmiller, M. & Kussoy, M. 1983 Hot-wire and laser doppler anemometer measurements in a supersonic boundary layer. *AIAA Paper* 83-1723.

Spalart, P. 1988 Direct numerical simulation of a turbulent boundary layer up to $R_\theta = 1410$. *J. Fluid Mech.* **187**, 61–98.

Van-Driest, E. 1956 Problem of aerodynamic heating. *Aeronaut. Engng Rev.* **15**, 26–41.

Weirs, V. & Candler, G. 1997 Optimization of weighted ENO schemes for DNS of compressible turbulence. *AIAA Paper* 97-1940. Also V.G. Weirs PhD Thesis, University of Minnesota, 1998.

Wright, M. 2003 DPLR and CFD and code. NASA Ames Research Center, Moffett Field, CA.

Wu, M. & Martin, M. 2004 Direct numerical simulation of shockwave/turbulent boundary layer interaction. *AIAA Paper* 2004-2145.

Xu, S. & Martin, M. 2003 Assessment of inflow boundary conditions for compressible turbulent boundary layers. *AIAA Paper* 2003-3963.

Xu, S. & Martin, M. 2004 Assessment of inflow boundary conditions for compressible turbulent boundary layers *Phys. Fluids.* **16**, 2623–2639.